Climate Dynamics (2005) 24: 89–104
DOI 10.1007/s00382-004-0478-x

**Matthew Collins · The CMIP Modelling Groups (BMRC (Australia), CCC (Canada), CCSR/NIES (Japan), CERFACS (France), CSIRO (Austraila), MPI (Germany), GFDL (USA), GISS (USA), IAP (China), INM (Russia), LMD (France), MRI (Japan), NCAR (USA), NRL (USA), Hadley Centre (UK) and YNU (South Korea))**

# El Niño- or La Niña-like climate change?

Received: 16 December 2003 / Accepted: 27 August 2004 / Published online: 9 December 2004


**Abstract** The potential for the mean climate of the tropical Pacific to shift to more El Niño-like conditions as a result of human induced climate change is subject to a considerable degree of uncertainty. The complexity of the feedback processes, the wide range of responses of different atmosphere–ocean global circulation models (AOGCMs) and difficulties with model simulation of present day El Niño southern oscillation (ENSO), all complicate the picture. By examining the components of the climate-change response that projects onto the model pattern of ENSO variability in 20 AOGCMs submitted to the coupled model inter-comparison project (CMIP), it is shown that large-scale coupled atmosphere–ocean feedbacks associated with the present day ENSO also operate on longer climate-change time scales. By linking the realism of the simulation of present day ENSO variability in the models to their patterns of future mean El Niño-like or La Niña-like climate change, it is found that those models that have the largest ENSO-like climate change also have the poorest simulation of ENSO variability. The most likely scenario ($p = 0.59$) in a model-skill-weighted histogram of CMIP models is for no trend towards either mean El Niño-like or La Niña-like conditions. However, there remains a small probability ($p = 0.16$) for a change to El Niño-like conditions of the order of one standard El Niño per century in the 1% per year $CO_2$ increase scenario.

M. Collins
Hadley Centre for Climate Prediction and Research,
Met Office, FitzRoy Road, Exeter, EX1 3PB, UK
E-mail: matthew.collins@metoffice.gov.uk
Tel.: +44-1392-884110
Fax: +44-870-9005050

## 1 Introduction

Like many aspects of anthropogenically forced climate change, predictions of the future state of the climate of the tropical Pacific (under a given scenario of enhanced greenhouse gases and other radiatively active substances) are highly uncertain. Will sea surface temperatures warm uniformly across the basin? Will there be greater warming in the east in comparison to the west, or greater warming in the west relative to the east? Will the pattern of change be more complex than a simple zonal dipole or uniform warming? What will be the atmospheric response to patterns of SST change?

For the purpose of this study, we may define the terms "El Niño-like" and "La Niña-like" climate change to denote patterns of mean change (or trend) in the equatorial tropical Pacific, which resemble at the ocean surface and in the atmosphere, a present day El Niño or La Niña event. Such trends in mean climate are of importance because of the potential for quasi-permanent changes in global climate, akin to those associated with present day El Niño southern oscillation (ENSO) variability. Phenomena as diverse as the stabilization of the thermohaline circulation (Latif et al. 2000), changes in tropical cyclone tracks (McDonald et al. 2004) and the possible death of the Amazon rainforest (Cox et al. 2000, 2004) have all been related to ENSO-like mean changes. Changes in ENSO variability about a new mean state (Timmermann et al. 1999; Collins 2000) further complicate the picture but are not considered here.

Uncertainty arises partly because of the conflicting theories about the mechanisms for mean climate change in the region (Clement and Seager 1999; Knutson and Manabe 1995; Cane et al. 1997; Pierrehumbert 1995) that almost certainly involve complex cloud feedbacks (Senior 1999; Meehl et al. 2000) and partly because AOGCMs have produced a wide range of responses

(Meehl and Washington 1996; Knutson and Manabe 1998; Noda et al. 1999). There have been some suggestions of a real El Niño-like shift/trend in recent times, evident in both physical and biological indicators (Graham 1994; Trenberth and Hurrell 1994; Guilderson and Schrag 1998; Ebbesmeyer et al. 1991), although it is perhaps hard to separate the "signal" of any change from the "noise" of ENSO variability. Nevertheless, the IPCC third assessment report (Chap 9, Cubasch et al. 2001) did conclude that "Recent trends for surface temperature to become more El Niño-like in the tropical Pacific, ..., are projected to continue in many models".

Given a "perfect" model of the Earth system, and assuming the response to be predictable in the sense that for a relatively weak forcing (in comparison with e.g. glacial-interglacial cycle) associated with commonly used scenarios of future greenhouse gases there are no hysteresis effects or strong sensitive dependence on initial conditions, then we might make reliable predictions of tropical Pacific climate change under those given forcing scenarios. However, models are not perfect. For example, there are known systematic problems with cold biases in mean SSTs in the equatorial regions in many models (e.g. Meehl et al. 2000). Likewise, models exhibit varying degrees of success in simulating the main amplitude and frequency characteristics of the ENSO cycle (AchutaRao and Sperber 2002), the physics of which might be considered to be implicated in future climate change (as seen in Jin et al. 2001). We can strive to improve models and increase our understanding of the physical processes involved in tropical climate change (e.g. Sun and Liu 1996), yet there are considerable pressures from governments and other bodies to provide quantitative predictions of climate change to inform adaptation and mitigation policies. Just as is the case with short-term weather forecasting, we are required to make projections using imperfect models. How must we proceed?

**Table 1** Fraction of variance explained by the leading EOF of each CMIP2 model control simulation surface air temperature (SAT) in the region 120°E–90°W, 10°S–10°N

| Model/group | Variance explained (%) |
|---|---|
| BMRC | 44 |
| CCC | 42 |
| CCSR/NIES | 58 |
| CERFACS | 61 |
| CSIRO | 49 |
| MPI—ECHAM3 | 37 |
| MPI—ECHAM4 | 59 |
| GFDL | 19 |
| GISS | 63 |
| IAP | 37 |
| INM | 57 |
| LMD | 44 |
| MRI | 57 |
| NCAR—CSM | 42 |
| NCAR—WM | 32 |
| NRL | 26 |
| PCM | 59 |
| UKMO—HadCM3 | 69 |
| UKMO—HadCM2 | 62 |
| YONU | 19 |
| Observations | 72 |

SAT was first interpolated onto the Hadley Centre model grid and land areas masked. Also shown is the variance explained by the leading EOF of the HadISST1 reconstruction of historical sea surface temperatures (Rayner et al. 2004)

Here, two steps are employed to quantify the uncertainty in current projections of climate change:

1. An ensemble of model simulations is employed and the prediction is quantitative in terms of the probability of a particular pattern of either El Niño or L Niña-like climate change.
2. Not all models are considered equal i.e. the better models are up-weighted and the poorer models are down-weighted in the prediction distributions, respectively.

The second step requires some quantitative measure of "model skill", which can be related (as objectively as possible) to the prediction variable in question. Together with the first step, this will allow us to move forward from statements such as "some models produce an El Niño-like warming, some models do not" to "there is a 16% chance of a warming trend similar to an average El Niño over the next 100 years". As pointed out by Allen and Stainforth (2002), in the absence of a perfect model this would seem the only sensible strategy for quantitative prediction. In order to reduce the uncertainty in climate prediction, we must first quantify it.

Ideally the ensemble of simulations should be large enough to systematically span the range of uncertainties associated with numerical climate prediction, e.g. resolution, poorly constrained parameters in parametrisation schemes, forcing scenarios, etc. Although some efforts have been initiated (Allen and Stainforth 2002; Murphy et al. (2004)), we are still far from possessing such an ensemble. Hence we may use an "ensemble of opportunity" provided by the coupled model intercomparison project (CMIP)—a database of the output of 20 different coupled atmosphere–ocean models. The different models are described in the CMIP web site (http://www-pcmdi.llnl.gov/cmip) and in Covey et al. (2003) and their ENSO variability is described in AchutaRao and Sperber (2002). Two simulations are provided from each model; (a) ~80 year control simulation with fixed levels of $CO_2$ and (b) ~80 year simulation in which $CO_2$ is increased from the control value at a rate of 1% per year compounded. This "scenario" is close enough to other established scenarios used by, e.g. the Intergovernmental Panel on Climate Change to provide a useful benchmark and to illustrate the method.

## 2 A method for producing probabilistic predictions of El Niño-like change

The method employed here is to represent the pattern of tropical Pacific climate change in each CMIP model in terms of the pattern of natural ENSO variability in that

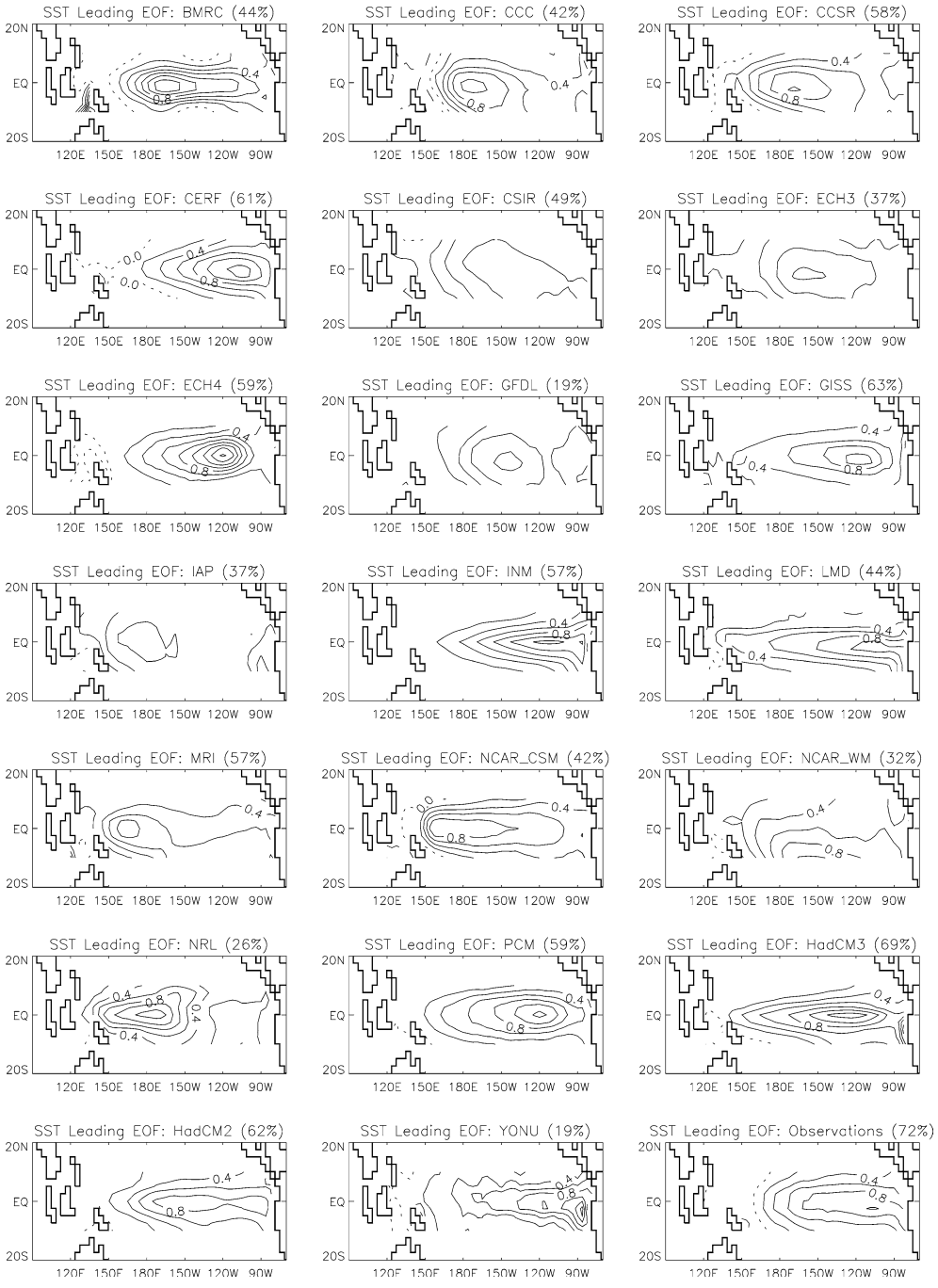


**Fig. 1** Spatial patterns of the leading EOF of de-seasonalised SAT in the region 120°E–90°W, 10°S–10°N for the CMIP2 control simulations and the observed SSTs. Model names are indicated and the fraction of interannual variance in each case in shown in *brackets*. Patterns are non-dimensional and have unit amplitude. The contour interval is 0.2, positive contours are shown as *solid lines*, the zero contour by the *dotted line* and negative contours *dashed*

model. This links the physical realism of some aspects of the model (e.g. the strength of the coupling between the atmosphere and the ocean) to its prediction of climate change. The following steps are performed.

## 2.1 Pre-processing of model fields

For each model and the observations (Rayner et al. 2004; Basnett and Parker 1997; Xie and Arkin 1997), the monthly mean surface air temperature (SAT), mean sea level pressure (MSLP) and precipitation (precip) are interpolated onto a 3.75° longitude by 2.5° latitude regular grid (identical to that used in the UKMO models) using bi-linear interpolation. Land areas in the SAT fields are masked to provide a proxy for SST. Anomalies are then computed with respect to a mean season cycle computed from the model control simulation. For the control simulation, a linear trend is removed at each grid-point in case of any model drifts. No trends are removed from the 1% per year experiments. Because of a large non-linear trend in the YONU model, only the first half of the control is used. Also, because only a few months are available for the NRL model control simulation, the detrended 1% per year experiment was used to compute the ENSO variability patterns.

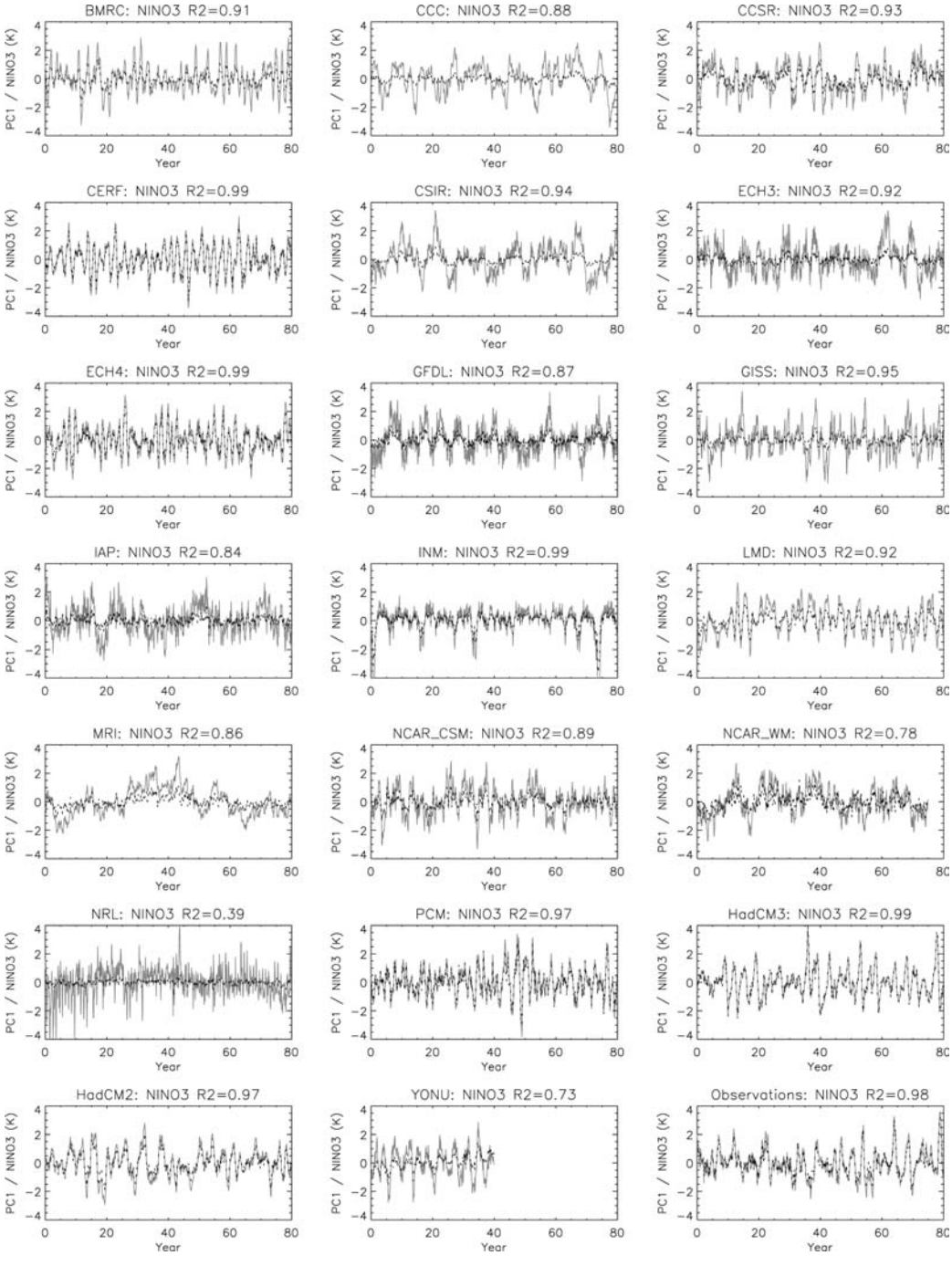


**Fig. 2** Normalised time coefficients of the leading EOF (*grey lines*) and un-normalised NINO3 anomalies (*dashed black lines*) for each model control simulation of the CMIP2 models and the observations. Correlation coefficients between each time series are indicated by the "R2" = text

## 2.2 Identification of the model ENSO cycle

For each model, the leading empirical orthogonal function (EOF) of SAT in the region 120°E–90°W, 10°S–10°N is computed from the de-trended control simulation anomalies. Table 1 gives the fraction of variance explained in each case and Fig. 1 shows the patterns. The spatial patterns, time coefficients of the leading EOF and NINO3 anomalies (Figs. 2, 3) are then examined to provide a subjective assessment of whether the leading EOF represented the model ENSO variability. This is judged to be true for all models.

## 2.3 Identification of the model "standard" El Niño event

The normalised (i.e. unit standard deviation) leading EOF time coefficient is then used to determine the

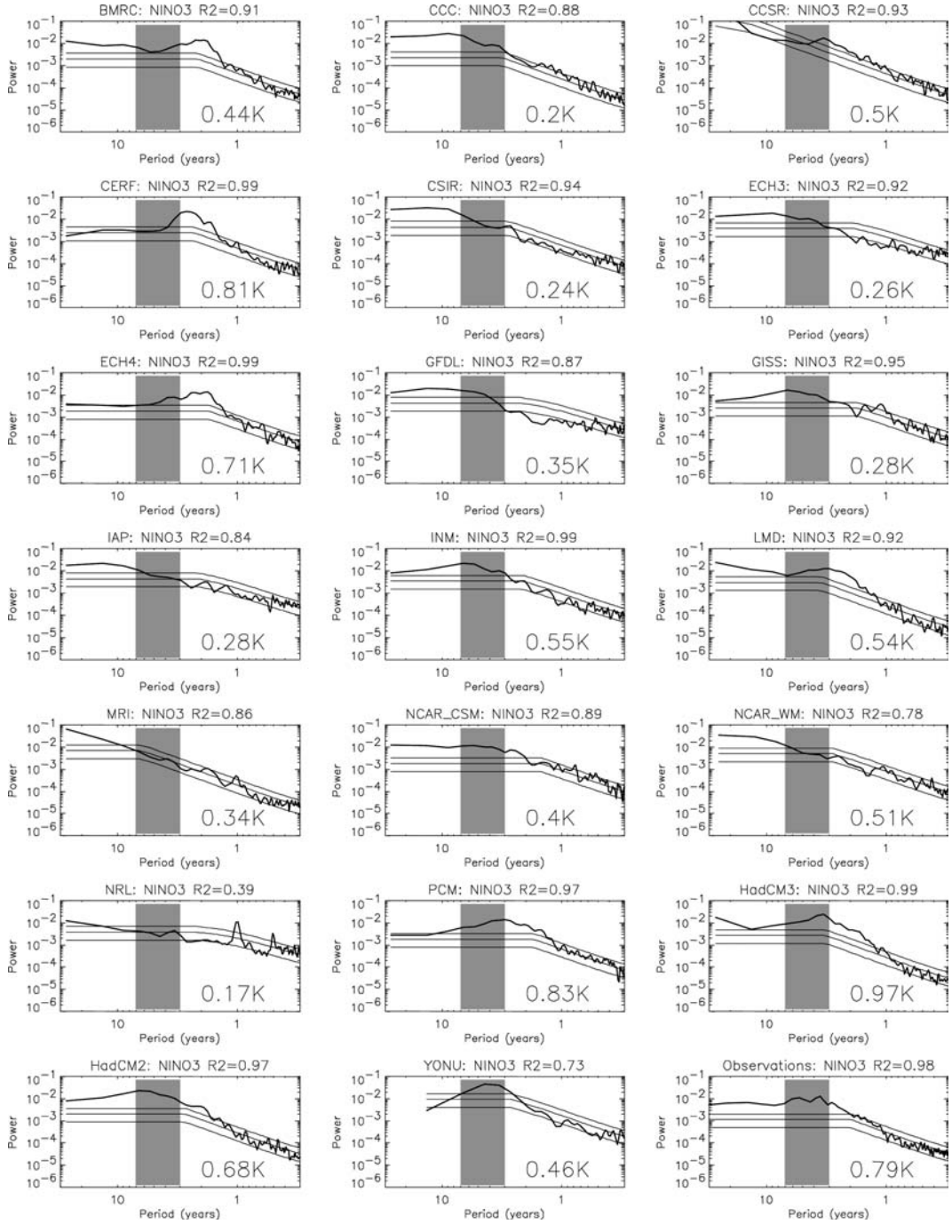


**Fig. 3** Power spectra of the normalised time coefficient of the leading EOF from each CMIP2 model control simulation (*think black lines*). The *thin black lines* indicate the power spectra of a fitted autoregressive process of order one: mean, 5- and 95%-tiles. The *shading* highlights the 3–7 year band where there is a relative excess of power in observed ENSO variability. The number in the *bottom right of each panel* is the standard deviation of the NINO3 anomalies from the model (and the observations). Annual and semi-annual peaks seen in the analysis of the NRL are due to the non-stationarity of the annual and semi-annual cycle in the 1% experiment which is used here because of an absence of control-simulation output

patterns of ENSO variability associated with SAT, MSLP and precip from the control simulations, e.g. $\mathrm{SAT} = \alpha\ \mathrm{ENSO}_{\mathrm{SAT}} + Q_{\mathrm{SAT}}$, where SAT is the space–time vector of SAT anomalies, $\alpha$ the time coefficient, $\mathrm{ENSO}_{\mathrm{SAT}}$ the time-invariant two-dimensional pattern and $Q_{\mathrm{SAT}}$ is a space–time residual. The resulting patterns; $\mathrm{ENSO}_{\mathrm{SAT}}$, $\mathrm{ENSO}_{\mathrm{MSLP}}$ and $\mathrm{ENSO}_{\mathrm{precip}}$ (Figs. 4, 5, 6) thus represent the spatial pattern of a one-standard deviation model El Niño event.

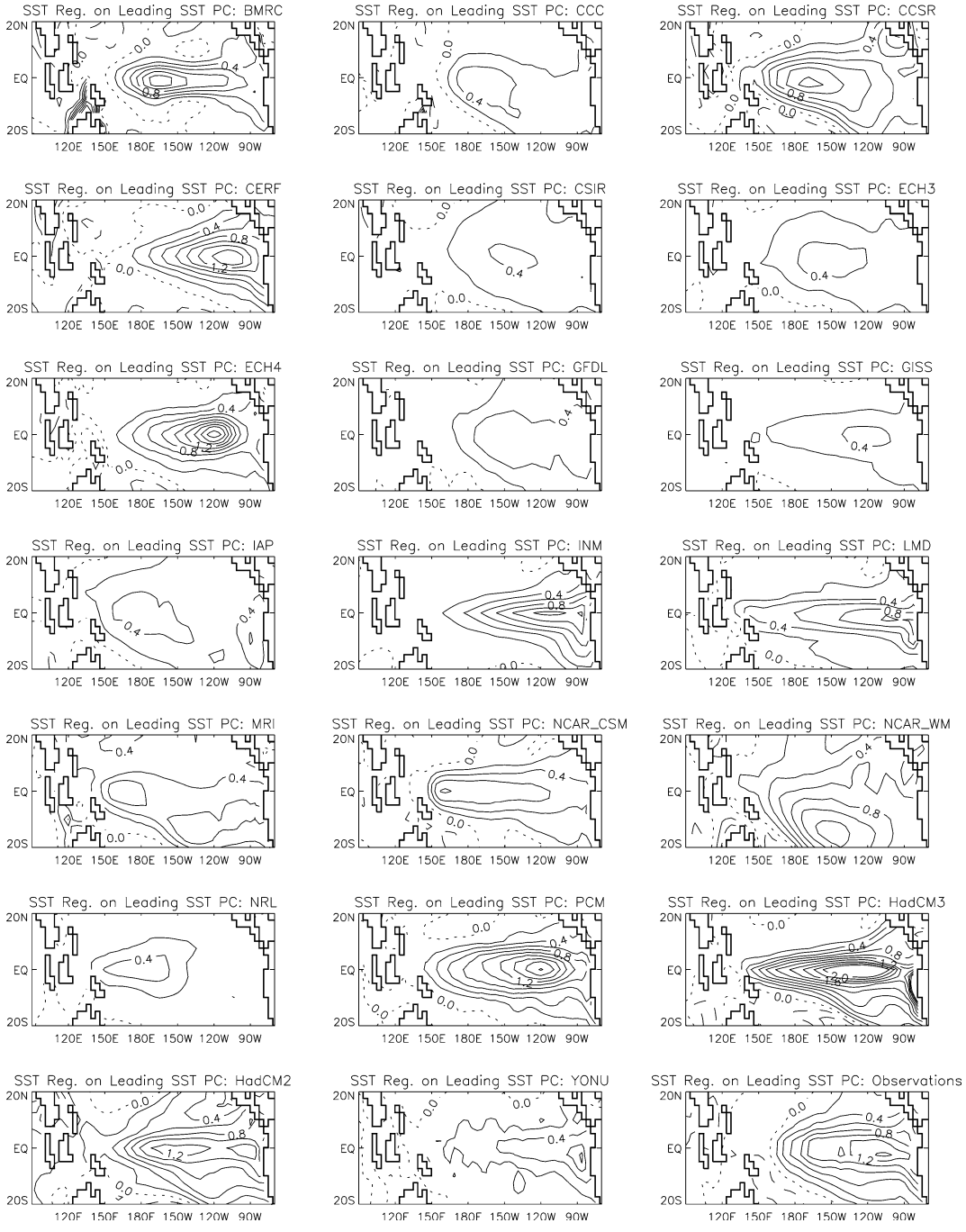


**Fig. 4** The SAT pattern corresponding to the CMIP2 models and the observed "standard El Niño event". Patterns are obtained by regressing the de-seasonalised SAT onto the normalised time coefficient of the leading EOFs of near-equatorial SAT shown in Fig. 1. Hence the patterns are very similar to those shown in Fig. 1 but now have a physical amplitude. The contour interval is 0.2 K, positive contours are shown as *solid lines*, the zero contour by the *dotted line* and negative contours by *dashed lines*

## 2.4 Projection of climate change trends onto model ENSO variability

Linear trends in de-seasonalised, SAT, MSLP and precip (Figs. 7, 8, 9) are then computed from the CMIP model 1% per year experiments and used in a further regression analysis: $\mathrm{Trend_{SAT}} = \beta_{\mathrm{SAT}}\ \mathrm{ENSO_{SAT}} + R_{\mathrm{SAT}}$, where $\mathrm{Trend_{SAT}}$ is a two-dimensional time-invariant pattern, $\beta_{\mathrm{SAT}}$ the regression coefficient and $R_{\mathrm{SAT}}$ is a two-dimensional residual. Thus $\beta_{\mathrm{SAT}}$, $\beta_{\mathrm{MSLP}}$ and $\beta_{\mathrm{precip}}$ are the amplitudes of trends in SAT, MSLP and precip expressed in terms of the particular models' pattern of ENSO variability and associated large-scale coupled atmosphere–ocean feedbacks. Linear trends

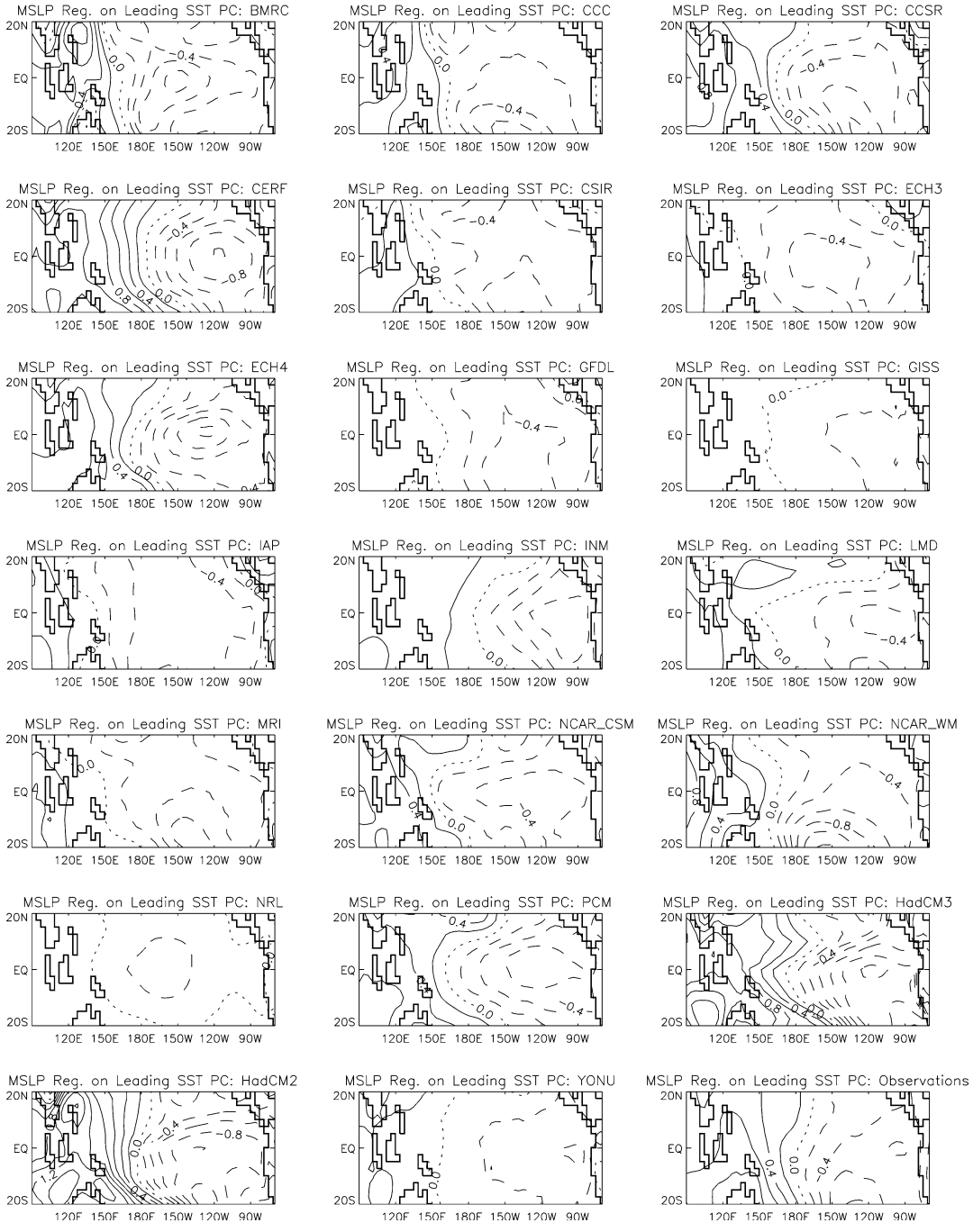


**Fig. 5** As in Fig. 4 but for MSLP anomalies (hPa) regressed onto the normalised time coefficient of the leading EOF of SAT. Contour interval 0.2 hPa

were found to be adequate in capturing the main features of the climate-change signals in the models (see, e.g. Fig. 9.3 of IPCC third assessment report, Chap. 9, Cubasch et al. 2001).

The β coefficients for each variable are numerically equal to the pattern correlation between the model trend pattern and the model pattern of ENSO variability normalised by the ratio of the standard deviation of the ENSO pattern and the trend pattern (Table 2). By examining these values, it is possible to assess if a large β is due to a strong similarity between the trend and the ENSO variability or due to large spatial variability of the trend pattern or a weak model ENSO. By projecting the climate-change signal in this way, it is possible to compare all models systematically, alleviating many of the errors associated

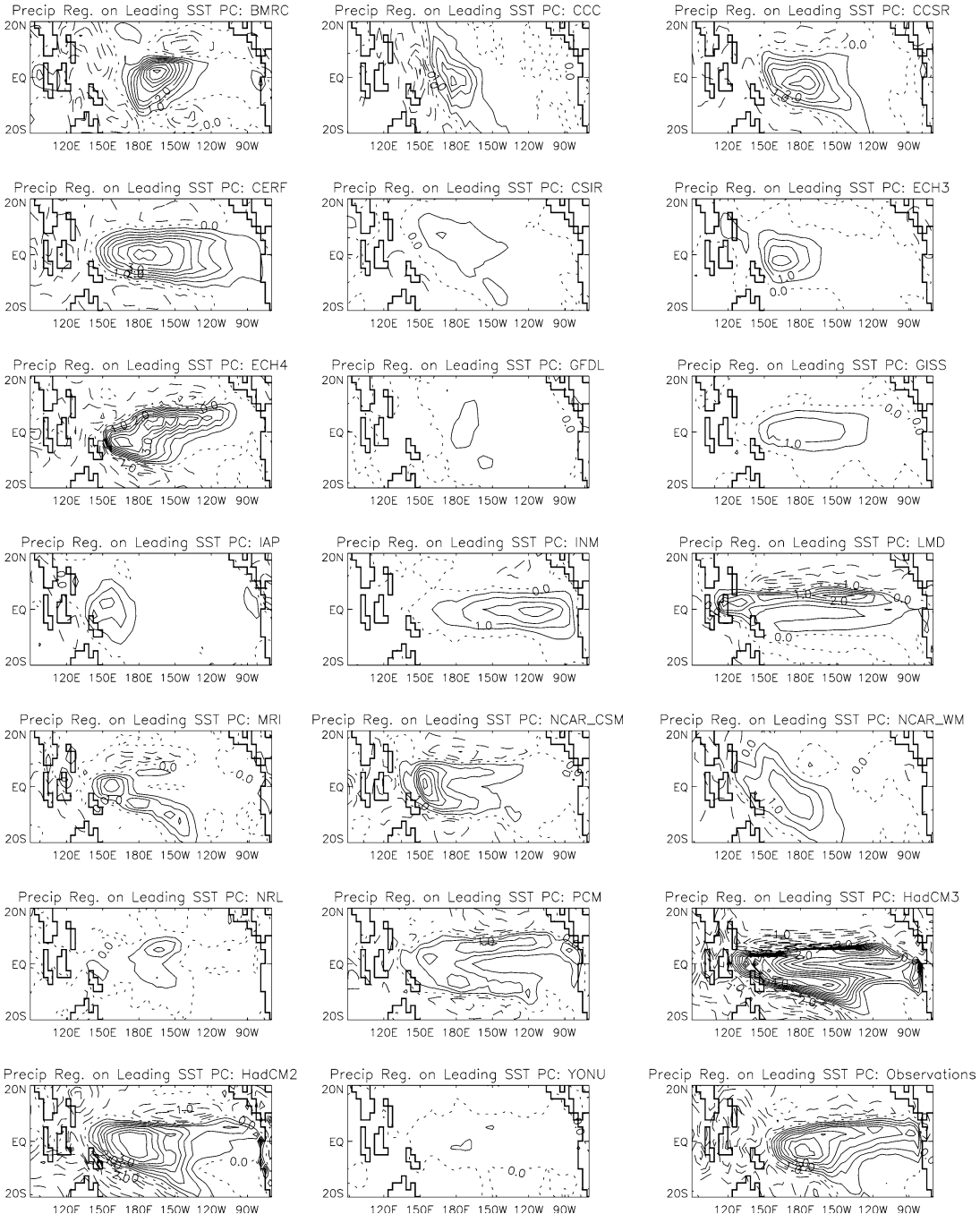


**Fig. 6** As in Fig. 4 but for precip anomalies (mm/day) regressed onto the normalised time coefficient of the leading EOF of SAT. Contour interval 0.5 mm/day

with mean climate and ENSO variability (e.g. the double ITCZ, too frequent ENSO events, too weak ENSO events, etc.) that would swamp any normal grid-point by grid-point comparison and amalgamation of model projections.

βs are shown in Fig. 10 and crucially reveal linear relationships between SAT, MSLP and precip trend patterns on century time scales. Hence, when the SAT trend projects onto the model El Niño, the associated MSLP and precip trends project onto the model El Niño teleconnection patterns with an amplitude consistent with that of the interannual variability (and likewise for a La Niña-like SAT change). The conclusion is that the coupled atmosphere–ocean processes that are responsible for determining the model ENSO cycle also operate on the long time scales of climate change. The implication is then that these large-scale coupled processes provide some constraints on the range of responses of the system.

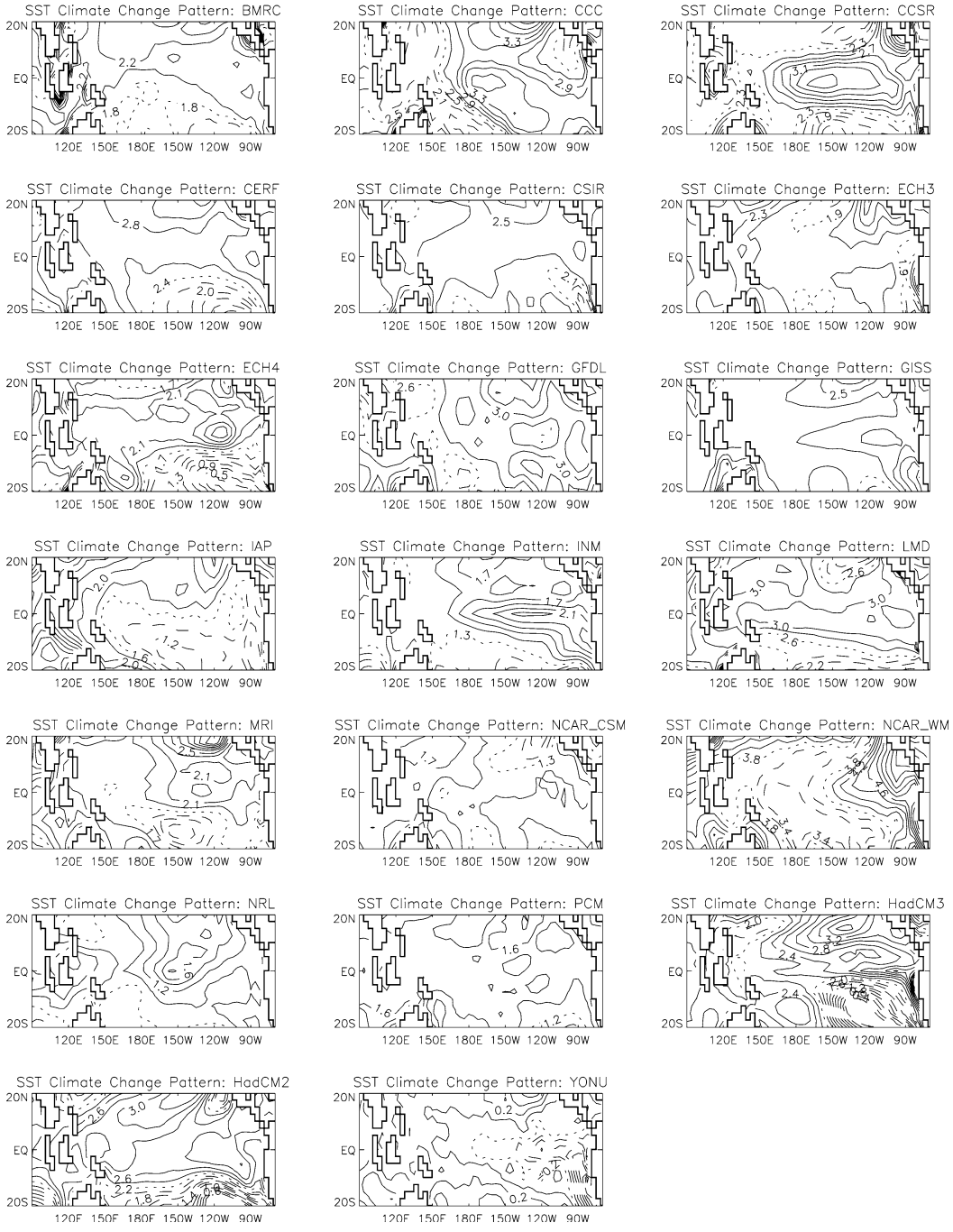


**Fig. 7** Patterns of SAT trend (K/century) from the CMIP2 1%/year experiments. The contour interval is 0.2 K/century and the contour lines are plotted such that positive contours show a trend greater than the mean for the region, the *dotted contour*shows this mean trend and the *dashed contours* show trends less than the mean for the region

## 3 A probabilistic prediction

If we take the CMIP ensemble projected in this way as the best estimate of current uncertainty in model estimates of climate change, then it is possible to produce a histogram of the range of ''ENSOness'' of future tropical Pacific climate change (Fig. 11a). The most probable ($p = 0.45$) outcome is for no large trend towards either El Niño or La Niña conditions. The second most probable outcome ($p = 0.20$) is for a trend of around ''1 standard El Niño/century'' in the 1% per year scenario—that is a trend pattern that would produce a mean climate change with the same pattern and magnitude as an El Niño event in 100 years. Equally probable ($p = 0.10$) is for either a 0.5 standard El Niño/century or a 0.5 standard La Nina/century. Also less probable ($p = 0.05$) is for

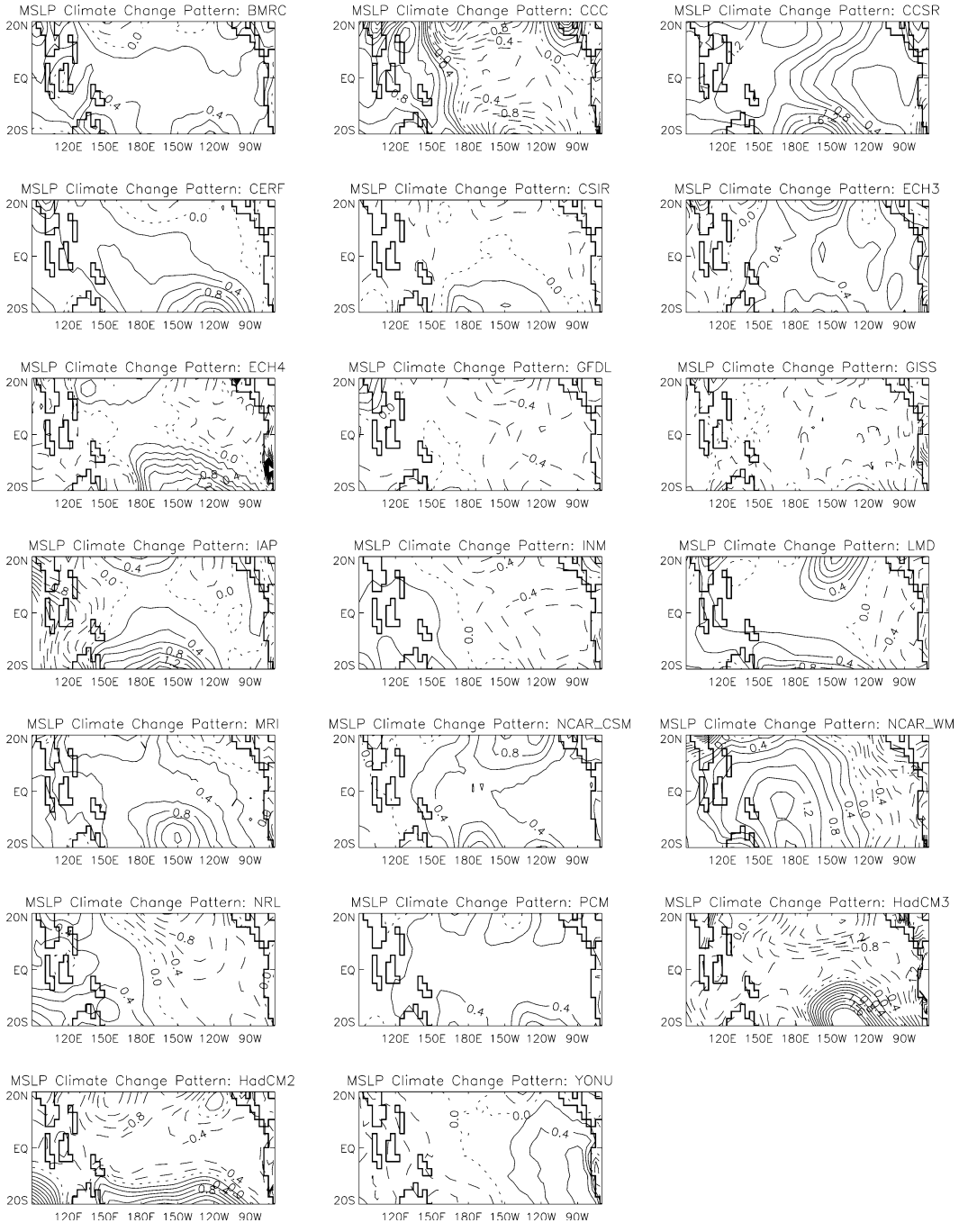


**Fig. 8** Patterns of MSLP trend (hPa/century) from the CMIP2 1%/year experiments. The contour interval is 0.2 hPa, positive contours are shown as *solid lines*, the zero contour by the *dotted line* and negative contours by *dashed lines*

$$\mathrm{ESI} = 1 - \mathrm{SQRT}\left[\frac{1}{6}\left(\begin{array}{c}(1-\gamma_{\mathrm{SAT}})^2 + (1-\gamma_{\mathrm{MSLP}})^2 + (1-\gamma_{\mathrm{precip}})^2 + \left|\frac{\mathrm{var(NINO3)} - \mathrm{var(NINO3_{obs})}}{\mathrm{var(NINO3_{obs})}}\right| + \\ \left|\frac{\mathrm{sp(NINO3)} - \mathrm{sp(NINO3_{obs})}}{\mathrm{sp(NINO3_{obs})}}\right| + \left|\frac{\mathrm{phase(NINO3)} - \mathrm{phase(NINO3_{obs})}}{\mathrm{phase(NINO3_{obs})}}\right|\end{array}\right)\right] \quad (1)$$

either a 2 standard El Niño/century or a 1.5 or 2 standard La Nina/century. Despite the relatively low probability of the extreme cases, these are situations which potentially can cause most disruption to society and it is therefore often more critical to determine their probability of occurrence.

Figure 11a gives all models equal weight regardless of their ability to simulate either mean climate or ENSO

**Table 2** Amplitude of ENSO-like climate change in the CMIP models

| Model | Amplitude of trend in terms of ENSO pattern ($\beta$) | | | Trend-ENSO pattern correlation | | | Ratio of trend pattern standard deviation and ENSO pattern standard deviation | | |
|---|---|---|---|---|---|---|---|---|---|
| | SAT | MSLP | Precipitation | SAT | MSLP | Precipitation | SAT | MSLP | Precipitation |
| BMRC | 0.11 | −0.01 | −0.05 | 0.11 | −0.02 | −0.07 | 0.95 | 0.48 | 0.65 |
| CCC | 2.19 | 2.10 | 2.05 | 0.85 | 0.89 | 0.87 | 2.59 | 2.36 | 2.34 |
| CCSR | 1.01 | 0.64 | 1.17 | 0.76 | 0.60 | 0.82 | 1.32 | 1.06 | 1.42 |
| CERF | 0.19 | 0.00 | 0.19 | 0.23 | 0.01 | 0.44 | 0.85 | 0.38 | 0.42 |
| CSIR | 0.44 | −0.42 | 0.04 | 0.35 | −0.48 | 0.03 | 1.28 | 0.88 | 1.58 |
| ECH3 | −0.58 | −0.98 | −0.34 | −0.35 | −0.65 | −0.34 | 1.67 | 1.51 | 1.01 |
| ECH4 | 0.35 | −0.15 | 0.43 | 0.23 | −0.16 | 0.41 | 1.49 | 0.90 | 1.04 |
| GFDL | 0.59 | 0.48 | 0.44 | 0.42 | 0.49 | 0.28 | 1.40 | 0.98 | 1.58 |
| GISS | 0.57 | 0.99 | 0.94 | 0.29 | 0.52 | 0.64 | 1.93 | 1.91 | 1.46 |
| IAP | −2.40 | −1.66 | −1.15 | −0.81 | −0.76 | −0.47 | 2.95 | 2.18 | 2.46 |
| INM | 0.86 | 0.77 | 0.96 | 0.79 | 0.85 | 0.86 | 1.09 | 0.91 | 1.12 |
| LMD | 0.54 | 0.52 | 0.70 | 0.40 | 0.40 | 0.58 | 1.36 | 1.31 | 1.21 |
| MRI | −0.53 | −0.71 | −0.80 | −0.34 | −0.53 | −0.52 | 1.59 | 1.35 | 1.54 |
| NCAR—CSM | −0.14 | −0.50 | −0.10 | −0.21 | −0.67 | −0.13 | 0.68 | 0.75 | 0.74 |
| NCAR—WM | −0.35 | 0.20 | −0.45 | −0.22 | 0.10 | −0.27 | 1.61 | 1.92 | 1.66 |
| NRL | 0.81 | 1.44 | 0.64 | 0.35 | 0.43 | 0.22 | 2.29 | 3.34 | 2.89 |
| PCM | 0.06 | −0.11 | 0.03 | 0.17 | −0.34 | 0.06 | 0.33 | 0.33 | 0.59 |
| HadCM3 | −0.03 | −0.06 | −0.35 | −0.02 | −0.06 | −0.29 | 1.26 | 0.97 | 1.22 |
| HadCM2 | 0.34 | 0.02 | 0.29 | 0.19 | 0.03 | 0.34 | 1.77 | 0.67 | 0.85 |
| YONU | −1.73 | −1.71 | −1.94 | −0.77 | −0.88 | −0.75 | 2.25 | 1.94 | 2.59 |

Columns 1–3 show $\beta$ coefficients in the regression of the trend in surface air temperature (SAT), mean sea level pressure (MSLP) and precipitation onto the normalised patterns of ENSO variability of those variables (see text for the equations used). Columns 4–6 show the spatial correlation between the trend patterns in the 1%/year $CO_2$ simulations and the leading patterns of ENSO variability and columns 7–9 show the ratio of the spatial standard deviations of those patterns for the respective variables

variability. Ideally we would like to down-weight poor models and up-weight good models in the estimate of the climate-change histogram. Model "goodness" can be argued in terms of resolution, accuracy of numerical schemes, use of flux adjustment, etc., but here we require a more systematic and quantitative approach. As the ENSO-like patterns of climate change involve the large-scale coupled feedbacks associated with ENSO, we define an "ENSO Simulation Index" (ESI) for each model: where SQRT is the square-root operator, $\gamma_{SAT}$, $\gamma_{MSLP}$ and $\gamma_{precip}$ are the regression coefficients of the model ENSO spatial variability patterns onto the observed spatial variability patterns (calculated in the same way as the β coefficients above), NINO3 and $NINO3_{obs}$ are the model and observed monthly NINO3 anomalies, var is the variance operator, sp an operator which gives the ratio of the spectral power in the 3–7 years period band to the spectral power at all other frequencies (the relative periodicity of the model ENSO cycle) and phase is an operator which gives the ratio of the December–February variance over the June–August variance, measuring the phase locking to the annual cycle. The ESI is one for a perfect simulation of ENSO and zero for a very poor simulation of ENSO.

The ESI for the CMIP model control simulations is shown in Fig. 11b against the ENSOness measure of the pattern of climate change in the model 1% per year experiments. It is clear that those models that have the best simulation of ENSO also have the smallest amplitude El Niño- or La Niña-like pattern of climate change. Those models with the largest amplitude response generally have a lower ESI and should therefore be down-weighted in the response histogram. The ESI-weighed histogram of the probability of El Niño- or La Niña-like climate change is shown in Fig. 13a. While not changing in overall shape in comparison to the unweighted histogram, the most likely no-trend case increases in likelihood ($p = 0.59$) and the extreme cases decrease in likelihood dropping below the 5% level. The second most likely pattern ($p = 0.16$, less likely than in the unweighted case) of response is for a 1 standard El Niño/century pattern of change.

Exploiting one further aspect of the method employed here, the spatial pattern of the trends associated with the $p = 0.16$ case can be found by examining the 1 standard El Niño patterns found using the above regression technique on the observed SST, MSLP and precip (Fig. 12). This technique thus produces a transfer function between the model patterns of change and the observed variability, in which we can have more confidence.

## 4 Sensitivity to the definition of model skill

The choice of ESI is somewhat subjective, although the definition used in the study is designed to evaluate the main characteristics of ENSO and its teleconnections, i.e. the spatial patterns, the amplitude, the frequency spectrum and the phase locking to the annual cycle. It is impossible to explore all possible definitions of ESI, but

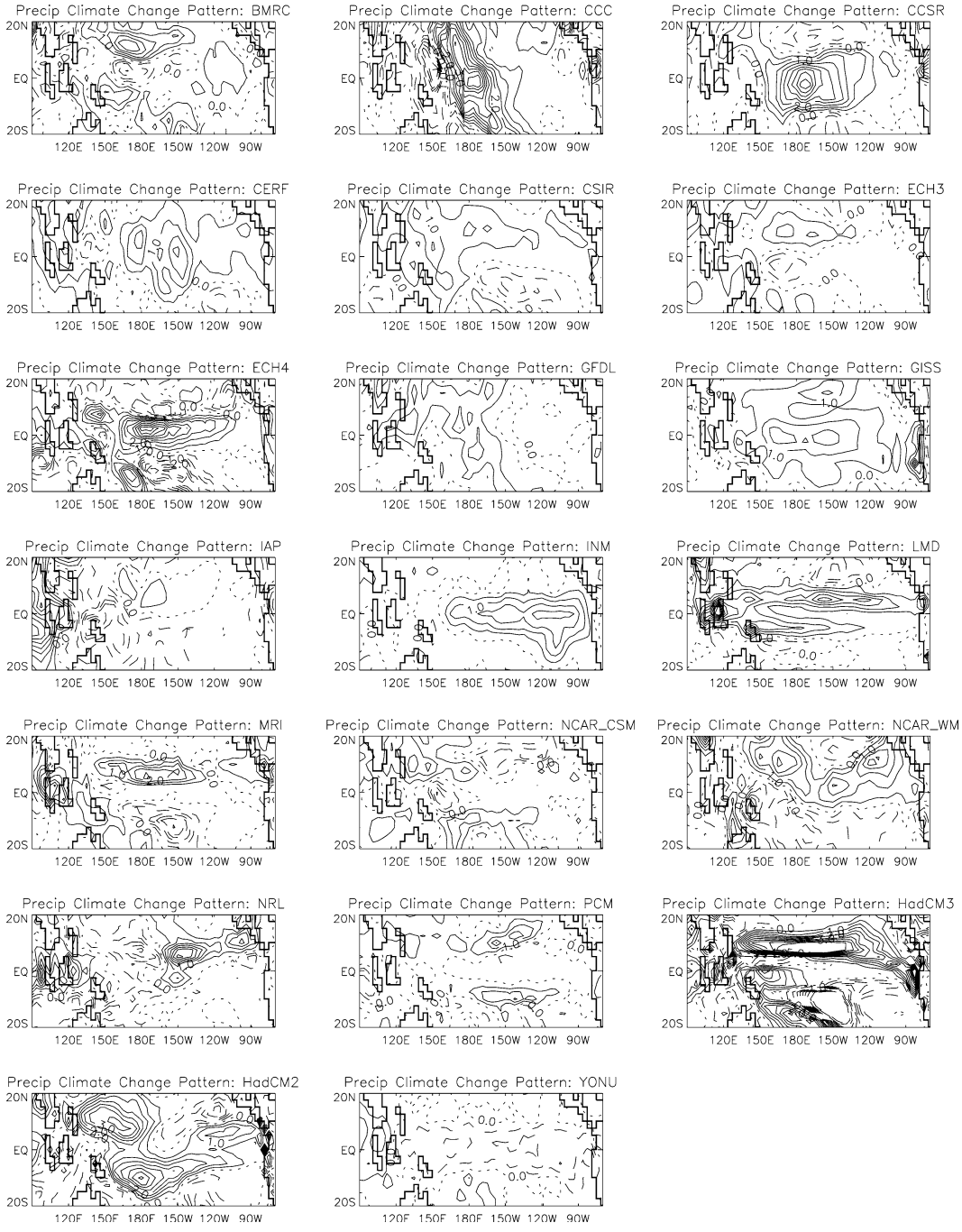


**Fig. 9** Patterns of precip trend ((mm/day)/century) from the CMIP2 1%/year experiments. The contour interval is 0.5 (mm/day)/century, positive contours are shown as *solid lines*, the zero contour by the *dotted line* and negative contours by *dashed lines*

it is possible to explore the sensitivity of the main results of the study to some obvious changes. The ''standard'' ESI is defined in Eq. 1. Five further definitions were applied:

ESI0 Standard definition
ESI1 Replace the regression coefficients in the first three terms with spatial correlation coefficients
ESI2 Remove the SQRT operator
ESI3 Use 2–8 years in the sp operator
ESI4 Use 4–6 years in the sp operator
ESI5 Add extra terms of the form $(1-\gamma_{\mathrm{MEAN\ SAT}})^2$

In ESI5 the extra terms quantify the skill of the model in producing mean conditions, although we should note that because some models employ flux-corrections, in those aspects of the mean climate are imposed and the skill will be artificially enhanced.

The resulting weighted histograms of ''ENSOness'' of future trends are shown in Fig. 13. It is clear that

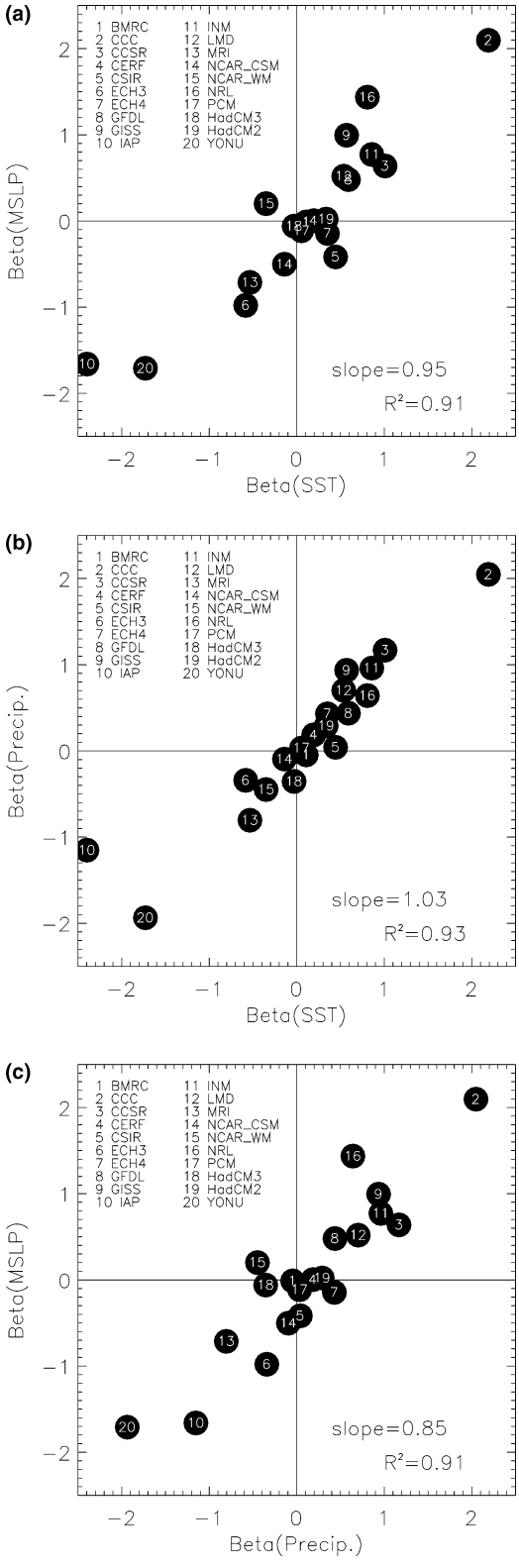


these different definitions of the ESI do not impact greatly on the main results set out in the main paper, i.e. the probability of the "no change" case is increased and the probability of the more extreme cases is reduced in comparison with the unweighted distribution.

◀

**Fig. 10** The amplitudes ($\beta$s) of trends in SAT, MSLP and precip from the 1%/year CMIP model experiments expressed in terms of the pattern of ENSO variability in the corresponding model control simulations (see text for more details). A $\beta_{SAT}$ of one indicates e.g. a SAT trend of one model standard El Niño event/century, a $\beta_{SAT}$ of $-1$ a model standard La Niña event/century etc. **a** $\beta_{SAT}$ versus $\beta_{MSLP}$, **b**$\beta_{SAT}$ versus $\beta_{precip}$, **c** $\beta_{precip}$ versus $\beta_{MSLP}$. The $R^2$ values indicate the correlation coefficients in each case. The linear relationships indicate that e.g. when the SAT trend projects onto the model El Niño patten, the associated MSLP and precip trends project onto the model El Niño teleconnection patterns with an amplitude consistent with interannual ENSO variability. The large-scale coupled atmosphere–ocean processes that determine the model ENSO variability are also active on longer time scales

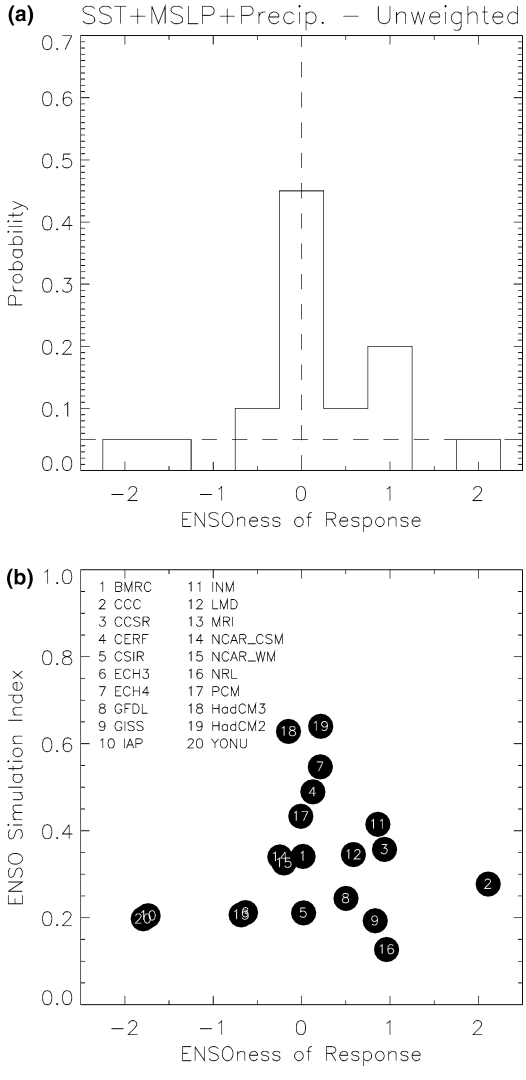


**Fig. 11** **a** Un-weighted histogram of the "ENSOness" of the pattern of climate change in the CMIP 1%/year experiments. The ENSOness is defined as the average of the $\beta_{SAT}$, $\beta_{MSLP}$ and $\beta_{precip}$ for each model (Fig. 10) and the histogram is normalised to give probability values. A bin size of 0.5 is used with bins centered on 0, $\pm 0.5$, $\pm 1$, etc. **b** ENSOness measure against ESI for the CMIP models. Those models with the more realistic ENSO cycle tend to have a smaller amplitude trend towards either El Niño-like or La Niña-like change

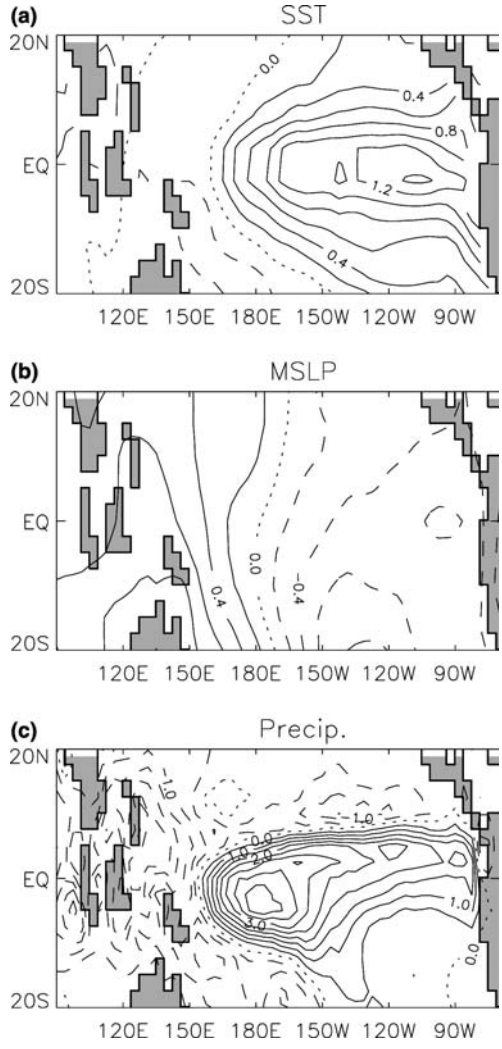


**Fig. 12** Patterns of a 1 standard El Niño event/century derived from observations. **a** SAT (K), **b** MSLP (hPa) and **c** precip (mm/day). These patterns have a 16% chance of occurring in the CMIP2 1%/year scenario according to the weighted histogram shown in Fig. 13(a)

The definition of any model skill index used in a weighted-ensemble prediction will be open to criticisms of subjectivity. Ultimately, we require measures which are formally related to the likelihood of the predictand variable of interest—information, which may be gleaned from past observations of climate change, either historical or palaeo. An uncomfortable consequence of this method is that such observations may not be of high-enough quality or may not even be available. The pragmatic approach is therefore to examine the sensitivity of the probabilistic prediction to variations in the definition of skill.

## 5 Discussion and conclusions

In terms of the questions set out in the first paragraph of the introduction, the global database of complex coupled atmosphere–ocean models suggests that the most likely scenario (as revealed in Figs. 11 and 13 for both the unweighted and weighted distributions) is for no large-amplitude change towards mean El Niño-like or La Niña-like conditions. In terms of the paradigm for climate change, in which the signal is manifested as changes in the frequency or residence times of model variability (Corti et al. 1999), this appears not to be the case here.

The study has shown that by critically and quantitatively examining the model physical processes (in this case the large-scale atmosphere–ocean, or "dynamical thermostat" feedbacks, following Jin et al. 2001) in an ensemble of models it is possible to produce quantitative probabilistic forecasts of future climate. This is a first step and many improvements can and should be made. For example, other patterns/modes are also evident in the climate-change trends (see Figs. 7, 8, 9) and those may obscure the ENSO-like pattern. Subsequent studies should identify higher-order modes in order to explain a greater fraction of the climate-change patterns. In addition, variables which determine other feedbacks associated with clouds, radiation and evaporation may be considered (Sun and Liu 1996; Li et al. 2000; Jin et al. 2001).

While the CMIP models produce a wide range of responses, they are unlikely to even represent the true level of uncertainty as many of the models share components, parametrisation schemes, etc. and are therefore not completely independent. A reduction of the effective degrees of freedom in the weighted histogram of future states (Fig. 13) would, most likely, result in a reduction of the probability of no trend and an increase in the probability of more ENSO-like climate change. It remains a considerable challenge not only to improve models but also to produce ensembles of climate-change experiments that span the true range of uncertainty. Ensembles with perturbed parameters in the physical parametrisation schemes (Allen and Stainforth 2002) may be one possible solution, as may "stochastic physics" (Buizza et al. 1999). In addition, it must again be stressed that it is crucial to link the integrity of the model simulation of present day climate and climate change to the future predictions in a quantitative way.

**Acknowledgements** This study could not have been performed without the contributions of all the CMIP participants and the excellent work of the PCMDI CMIP team. This work was supported by the UK Department of the Environment, Food and Rural Affairs under Contract PECD/7/12/37 and by the UK National Environment Research Council under the COAPEC programme.

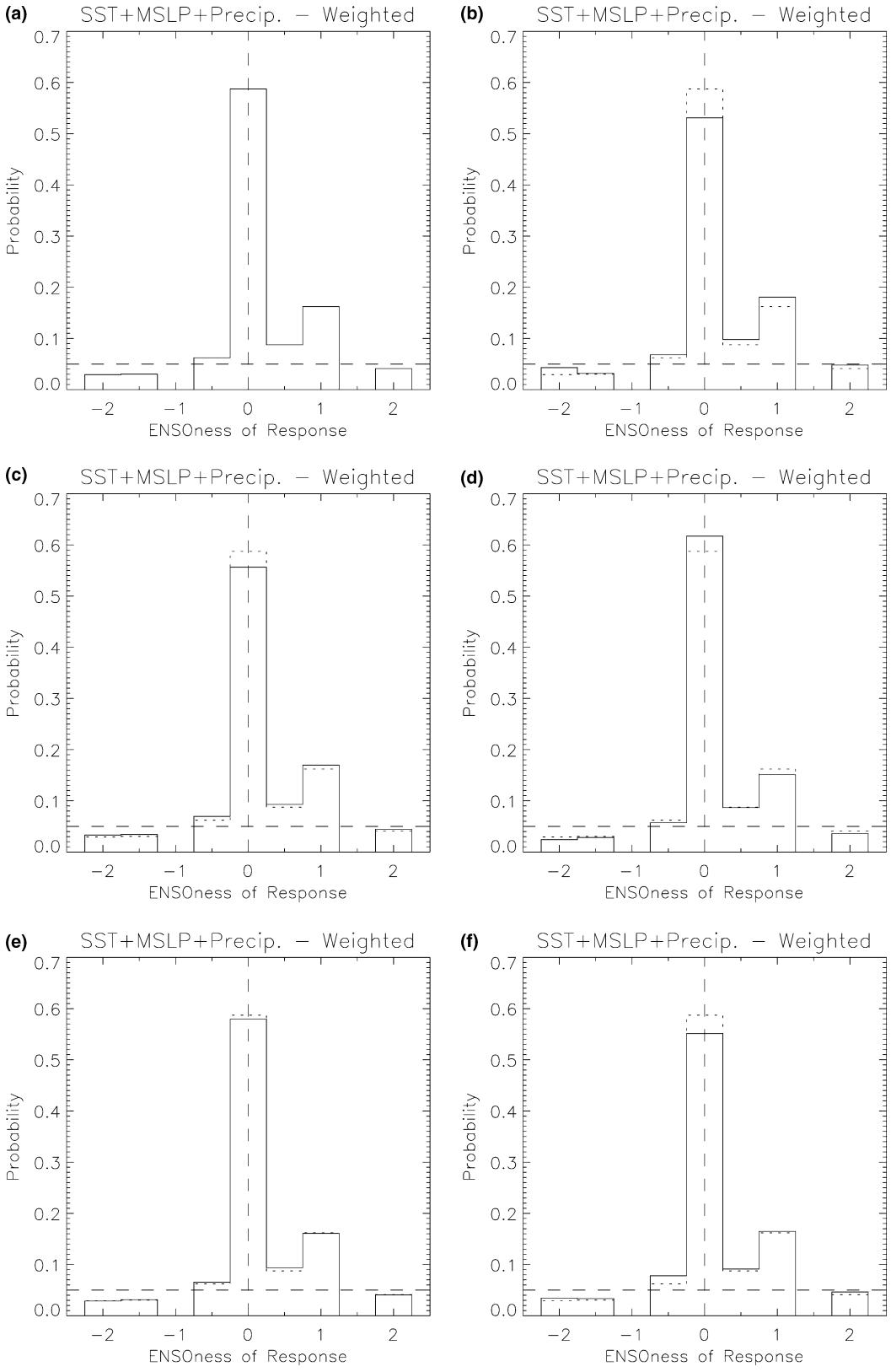


**Fig. 13** Weighted histograms of ENSOness of future mean trends in the tropical Pacific in the CMIP2 1%/year scenario. The weighting in each case is according to different definitions of the ENSO simulation index set out in the text. **a** ESI0, **b** ESI1, **c**ESI2, **d** ESI3, **e** ESI4, **f** ESI5

## References


Achutarao K, Sperber KR in collaboration with the CMIP modeling groups (2002) Simulation of the El Niño southern oscillation: results from the coupled model intercomparison project. Clim Dyn 19:191–209

Allen MR, Stainforth DA (2002) Towards objective probabilistic climate forecasting. Nature 419:228

Basnett TA, Parker DE (1997) Development of the global mean sea level pressure data set GMSLP2. Hadley Centre Climate Research Technical Note CRTN 79

Buizza R, Miller M, Palmer TN (1999) Stochastic representation of model uncertainties in the ECMWF EPS. Quart J R Met Soc 125:2887–2908

Cane MA, Clement AC, Kaplan A, Kushnir Y, Pozdnyakov D, Seager SE, Zebiak SE, Murtugudde R (1997) Twentieth century sea surface temperature trends. Science 275:957–960

Clement A, Seager R (1999) Climate and tropical oceans. J Clim 12:3383–3401

Collins M (2000) Understanding uncertainties in the response of ENSO to greenhouse warming. Geophys Res Lett 27(21):3509–3513

Corti S, Molteni F, Palmer TN (1999) Signature of recent climate change in frequencies of natural atmospheric circulation regimes. Nature 398:799–802

Covey C, AchutaRao KM, Cubasch U, Jones P, Lambert SJ, Mann ME, Phillips TJ, Taylor KE (2003) An overview of the results of the coupled model intercomparison project. Global Planetary Change 37:103–133

Cox PM, Betts RA, Jones CD, Spall SA, Totterdell I (2000) Acceleration of global warming due to carbon cycle feedbacks in a coupled climate model. Nature 408:184–187

Cox PM, Betts RA, Collins M, Harris P, Huntingford C, Jones CD (2004) Amazon dieback under climate-carbon cycle projections for the 21st century. Theor Appl Climatol 78:137–156. DOI: 10.1007/s00704-004-0049-4

Cubasch U, Meehl GA et al (2001) The scientific basis. Contribution of working group I to the third assessment report of the Intergovernmental Panel on Climate Change. Cambridge University Press, Cambridge

Ebbesmeyer CC, Cayan DR, McLain DR, Nichols FH, Peterson DH, Redmond KT (1991). 1976 step in the Pacific climate: forty environmental changes between 1968–1975 and 1977–1984. In: Betancourt JL, Sharp VL (eds) Proceedings of the 7th annual Pacific climate (PACLIM) workshop, April 1990. California Department of Water Resources. Interagency Ecological Studies Program Technical Report 26

Graham NE (1994) Decadal-scale climate variability in the tropical and North Pacific during the 1970s and 1980s: observations and model results. Clim Dyn 10:135–162

Guilderson TM, Schrag D (1998) Abrupt shift in subsurface temperature in the tropical Pacific associated with changes in El Niño. Science 281:240–243

Jin F-F, Hu Z-Z, Latif M, Bengtsson L, Roeckner E (2001) Dynamical and cloud–radiation feedbacks in El Niño and greenhouse warming. Geophys Res Lett 28:1539–1542

Knutson TR, Manabe S (1995) Time-mean response over the tropical Pacific to increased $CO_2$ in a coupled ocean–atmosphere model. J Climate 8:2181–2199

Kuntson TR, Manabe S (1998) Model assessment of decadal variability and trends in the tropical Pacific ocean. J Climate 11:2273–2296

Latif M, Roeckner E, Mikolajewicz U, Voss R (2000) Tropical stabilization of the thermohaline circulation in a greenhouse warming simulation. J Climate 13:1809–1813

Li T, Hogan TF, Chang C-P (2000) Dynamic and thermodynamic regulation of ocean warming. J Atmos Sci 57:3353–3365

McDonald RE, Bleaken DG, Cresswell DR, Pope VD, Senior CA (2004) Tropical storms: representation and diagnosis in climate models and the impacts of climate change. Clim Dyn (in press). DOI:10.1007/s00382-004-0491-0

Meehl GA, Washington WM (1999) El Niño-like climate change in model with increased atmospheric $CO_2$concentrations. Nature 382:56–60

Meehl GA, Collins W, Boville B, Kiehl JT, Wigley TML, Arblaster JM (2000) Response of the NCAR climate system model to increased $CO_2$ and the role of physical processes. J Climate 13:1879–1898

Noda A, Yoshimatsu K, Yukimoto S, Yamahuchi K, Yamaki S (1999) Relationship between natural variability and $CO_2$-induced warming pattern: MRI AOGCM experiment. In: 10th symposium on global change studies, American Meteorological Society Publication

Pierrehumbert RT (1995) Thermostats, radiator fins, and the local runaway greenhouse. J Atmos Sci 52:1784–1806

Rayner NA, Parker DE, Horton EB, Folland CK, Alexander LV, Rowell DP, Kent EC, Kaplan, A (2004) Globally complete analyses of SST, sea-ice and night marine air temperature, 1871–2000. J Geophys Res (in press)

Senior CA (1999) Comparison of mechanisms of cloud–climate feedbacks in a GCM. J Climate 12:1480–1489

Sun, DZ, Liu, Z (1996) Dynamic ocean–atmosphere coupling: a thermostat for the tropics. Science 272:1148–1150

Timmermann A, Oberhuber J, Bacher A, Esch M, Latif M, Roeckner E (1999) Increased El Niño frequency in a climate model forced by future greenhouse warming. Nature 398:694–696

Trenberth KE, Hurrell JW (1994) Decadal atmosphere–ocean variations in the Pacific. Clim Dyn 9:303–319

Xie P, Arkin PA (1997) Global precipitation: a 17-year monthly analysis based on gauge observations, satellite estimates and numerical model outputs. Bull Am Met Soc 78:2539–2558